Ventricular–subventricular zone fractones are speckled basement membranes that function as a neural stem cell niche

Yuya Sato[a,†], Daiji Kiyozumi[a,‡], Sugiko Futaki[a,§], Itsuko Nakano[a], Chisei Shimono[a], Naoko Kaneko[b], Masahito Ikawa[c], Masaru Okabe[c], Kazunobu Sawamoto[b,d], and Kiyotoshi Sekiguchi[a,e,*]

[a]Laboratory of Extracellular Matrix Biochemistry, Institute for Protein Research, Osaka University, Suita, Osaka 565-0871, Japan; [b]Department of Developmental and Regenerative Biology, Nagoya City University Graduate School of Medical Sciences, Nagoya, Aichi 467-8610, Japan; [c]Department of Experimental Genome Research, Research Institute for Microbial Diseases, Osaka University, Suita, Osaka 565-0871, Japan; [d]Division of Neural Development and Regeneration, National Institute for Physiological Sciences, Okazaki, Aichi 444-8585, Japan; [e]Laboratory of Matrixome Research and Application, Institute for Protein Research, Osaka University, Suita, Osaka 565-0871, Japan

ABSTRACT **Neural stem cells (NSCs) are retained in the adult ventricular–subventricular zone (V-SVZ), a specialized neurogenic niche with a unique cellular architecture. It currently remains unclear whether or how NSCs utilize basement membranes (BMs) in this niche. Here, we examine the molecular compositions and functions of BMs in the adult mouse V-SVZ. Whole-mount V-SVZ immunostaining revealed that fractones, which are fingerlike processes of extravascular BMs, are speckled BMs unconnected to the vasculature, and differ in their molecular composition from vascular BMs. Glial fibrillary acidic protein (GFAP)-positive astrocytes and NSCs produce and adhere to speckled BMs. Furthermore, *Gfap-Cre*-mediated *Lamc1*$^{flox(E1605Q)}$ knockin mice, in which integrin-binding activities of laminins are specifically nullified in GFAP-positive cells, exhibit a decreased number and size of speckled BMs and reduced in vitro neurosphere-forming activity. Our results reveal niche activities of fractones/speckled BMs for NSCs and provide molecular insights into how laminin–integrin interactions regulate NSCs in vivo.**

Monitoring Editor
Yukiko Yamashita
University of Michigan

Received: May 11, 2018
Revised: Oct 23, 2018
Accepted: Oct 26, 2018

INTRODUCTION

Neurogenesis persists throughout life in two germinal regions of the adult mammalian brain: the ventricular–subventricular zone (V-SVZ) of the lateral ventricle and the subgranular zone of the hippocampus (Alvarez-Buylla and Lim, 2004). In both regions, astrocytes have been shown to act as neural stem cells (NSCs; Doetsch, 2003). In the V-SVZ, a subset of glial fibrillary acidic protein (GFAP)-expressing astrocytes, called type B cells, are NSCs. These NSCs generate transit-amplifying cells (type C cells), which in turn produce neuroblasts

This article was published online ahead of print in MBoC in Press (http://www.molbiolcell.org/cgi/doi/10.1091/mbc.E18-05-0286) on October 31, 2018.

Competing financial interests: K. Sekiguchi is a cofounder and stockholder of Matrixome. The other authors declare no potential conflicts of interest.

Present addresses: [†]Laboratory of Stem Cell and Neuro-Vascular Biology, Genetics and Developmental Biology Center, National Heart, Lung, and Blood Institute, National Institutes of Health, Bethesda, MD 20892; [‡]Department of Experimental Genome Research, Research Institute for Microbial Diseases and Immunology Frontier Research Center, Osaka University, Suita, Osaka 565-0871, Japan; [§]Department of Anatomy and Cell Biology, Osaka Medical College, Takatsuki, Osaka 569-8686, Japan.

Author contributions: Y.S. designed the study, performed the majority of the experiments and analyses, and wrote the paper; D.K. and S.F. produced the *Lamc1*^{cEQ} *and Lama5*^{fl} mice, respectively; C.S. provided recombinant α1β1 and α2β1 integrins; I.N. prepared frozen tissue sections; M.I. and M.O. provided technical assistance in generating the *Lama5*^{fl} *and Lamc1*^{cEQ} mice; N.K. and Ka.S. provided protocols for whole-mount V-SVZ immunostaining, discussed the data, and advised on the writing of the paper; Ki.S. conceived, designed, and supervised the study, analyzed the data, and wrote the paper.

*Address correspondence to: Kiyotoshi Sekiguchi (sekiguch@protein.osaka-u.ac.jp).

Abbreviations used: BM, basement membrane; BMP, bone morphogenic protein; BSA, bovine serum albumin; CSF, cerebrospinal fluid; Dcx, doublecortin; ECM, extracellular matrix; EdU, 5-ethynyl-29-deoxyuridine; FGF, fibroblast growth factor; GFAP, glial fibrillary acidic protein; LM, laminin; MAPK, mitogen-activated protein kinase; NSC, neural stem cell; PBS, phosphate-buffered saline; PECAM, platelet endothelial cell adhesion molecule; RGD, arginine–glycine–aspartic acid; TGF, transforming growth factor; V-SVZ, ventricular–subventricular zone.

(type A cells; Doetsch *et al.*, 1999). NSC behavior and fate are regulated by a balance of intrinsic and extrinsic cues that vary with physiological and pathological conditions (Silva-Vargas *et al.*, 2013).

A key determinant of NSC behavior is the NSC niche, a protective milieu of supporting cells, stem cells, and extracellular matrix (ECM; Riquelme *et al.*, 2008). Previous studies have elucidated the architecture of the V-SVZ niche as a whole and identified a subpopulation of type B cells with basal processes that make contact with blood vessels (Mirzadeh *et al.*, 2008; Shen *et al.*, 2008; Tavazoie *et al.*, 2008), suggesting a vascular niche for NSCs in the V-SVZ. Furthermore, some type B cells make direct contact with the lateral ventricle through apical processes that are interdigitated between ependymal cells. This configuration confers a pinwheel-like organization on the neurogenic region of the ventricular wall (Mirzadeh *et al.*, 2008). The direct interactions between type B cells, ependymal cells, and the lateral ventricle are indicative of niche activities for ependymal cells as well as for the cerebrospinal fluid (CSF) that fills the ventricular system (Riquelme *et al.*, 2008; Bjornsson *et al.*, 2015). Moreover, a variety of proteins, including bone morphogenic proteins (BMPs), noggin, fibroblast growth factors (FGFs), transforming growth factor (TGF)-α, and CXCL12, have been identified as niche factors that modulate neurogenesis (Lim *et al.*, 2000; Kokovay *et al.*, 2010; Silva-Vargas *et al.*, 2013; Bjornsson *et al.*, 2015). Although these studies clearly suggest the involvement of paracrine factors in the regulation of NSCs, the roles of ECMs in neurogenesis remain unclear.

Basement membranes (BMs) are thin sheetlike ECMs that act as niche factors for various stem cells by providing adhesive substrates and tissue stiffness or sequestering soluble factors (Hynes, 2009). To date, ~50 ECM proteins have been identified as BM components. Combinations of these proteins confer a wide range of receptor-binding repertoires and structures on BMs, thus providing customized microenvironments for individual cells (Manabe *et al.*, 2008). Deciphering the molecular compositions of BMs in stem cell niches is essential to understanding the regulation of stem cell functions in vivo. However, molecular profiling of BMs is challenging due to technical limitations in identifying the precise locations of individual BM proteins.

Two BM structures have been identified in the V-SVZ. Vascular BMs are the most abundant BMs produced by endothelial cells and smooth muscle cells (Yousif *et al.*, 2013). In addition, Mercier and colleagues reported another BM structure, fractones, as unique fingerlike processes of extravascular BMs that sequester intracerebroventricularly injected basic FGF and BMP-4/7 (Mercier *et al.*, 2002; Mercier and Douet, 2014; Kerever *et al.*, 2007; Douet *et al.*, 2012). Fractones were shown to contain laminins (LMs), types I and IV collagens, nidogen-1, and perlecan (Kerever *et al.*, 2007). Most of these proteins, except for type I collagen, are also components of vascular BMs, thus raising the possibility that fractones are extended from vascular BMs. However, because only a few proteins have been identified as constituting fractones and vascular BMs in the V-SVZ, it remains unclear whether fractones are simply extended structures of vascular BMs or functionally and structurally independent from vascular BMs. Moreover, the identity of the cells producing fractones in the V-SVZ is unknown, making it difficult to elucidate their physiological functions in vivo.

In this study, we comprehensively surveyed the molecular compositions of fractones and vascular BMs and found that the molecular composition of fractones differs from that of vascular BMs. Whole-mount V-SVZ immunostaining revealed that fractones are speckled BMs independent of the vasculature. GFAP-expressing adult NSCs/astrocytes, but not endothelial cells, are identified as producing LMs in speckled BMs. Furthermore, inactivation of LM integrin-binding activities in speckled BMs results in a decreased number and size of speckled BMs and severe impairment of neurosphere formation by NSCs, lending support to the notion that speckled BMs serve as an NSC niche.

RESULTS

Difference in protein compositions between vascular BMs and fractones

Two BM structures exist in the adult rodent V-SVZ: vascular BMs (LM and platelet endothelial cell adhesion molecule [PECAM]-positive tubules; >5 µm diameter; Figure 1, A and B, and Supplemental Figure S1) and fractones (extravascular LM-positive/PECAM-negative structures consisting of a stem and bulb; 1–3 µm diameter; Figure 1, A and B, and Supplemental Figure S1; Mercier *et al.*, 2002). To examine whether fractones are qualitatively different from vascular BMs, we performed immunohistochemical staining of adult mouse V-SVZs using a panel of antibodies against BM proteins (Manabe *et al.*, 2008). Vascular BMs and fractones were visualized by anti-panLM immunostaining and distinguished by their size as described previously (Mercier *et al.*, 2002). Among 12 LM subunits, vascular BMs were positive for LMα2/4/5, β1/2, and γ1, but negative for LMα1/3, β3, and γ2/3 (Figure 1, C and E). Besides LMs, vascular BMs contained type IV collagen α1/2 subunits, nidogen-1/2, perlecan, agrin, WARP, SMOC-1/2, netrin-4, endoGlyx-1, and leprecan (Figure 1, D and E, and Supplemental Figure S1). The molecular composition of fractones mostly overlapped with that of vascular BMs, as both contained LMα5, β1/2, and γ1, type IV collagen α1/2 subunits, nidogen-1/2, perlecan, agrin, SMOC-1/2, and netrin-4. However, LMα3 was detected only in fractones. Furthermore, LMα2/4 and WARP, which are representative of vascular BMs (Allen *et al.*, 2008; Yousif *et al.*, 2013), were absent in fractones. These results indicate that the molecular composition of fractones is similar, but not identical, to that of vascular BMs and raise the possibility that fractones are not extended from vascular BMs.

Fractones are speckled BMs unconnected to blood vessels

To investigate whether fractones are structurally independent of vascular BMs, we performed whole-mount V-SVZ immunostaining. The staining revealed numerous anti-panLM-immunoreactive speckles that appeared to be independent of the vasculature (Figure 2A; Supplemental Movie 1). These speckles were typically 1–3 µm in diameter and reminiscent of the fractones observed in brain sections (Figure 1). To establish whether the panLM-positive speckles were fractones, we assessed the molecular composition of the speckles by whole-mount V-SVZ immunostaining (Figure 2B). The speckles were positive for LMα3/5, LMβ1/2, LMγ1, type IV collagen, nidogen-1/2, perlecan, agrin, type VI collagen, and SMOC-1/2, but negative for LMα2/4 and WARP, similarly to the fractones observed in brain sections. These results demonstrate that the speckles observed in whole-mount V-SVZs are identical to the fractones observed in brain sections. Although fractones were named according to their fractal structure extending from vascular BMs (Mercier *et al.*, 2002), the name now appears to be misleading, based on our observations that fractones are structurally and molecularly distinct from vascular BMs. Fibrous BMs extending from the vascular BMs were occasionally visible around large blood vessels, which were characterized by surrounding vascular smooth muscle cells (Supplemental Figure S2), suggesting that the fibrous BMs correspond to the stems of fractones. Hereafter, we refer to these panLM-immunoreactive speckles as speckled BMs, because their molecular composition resembles that of typical BMs.

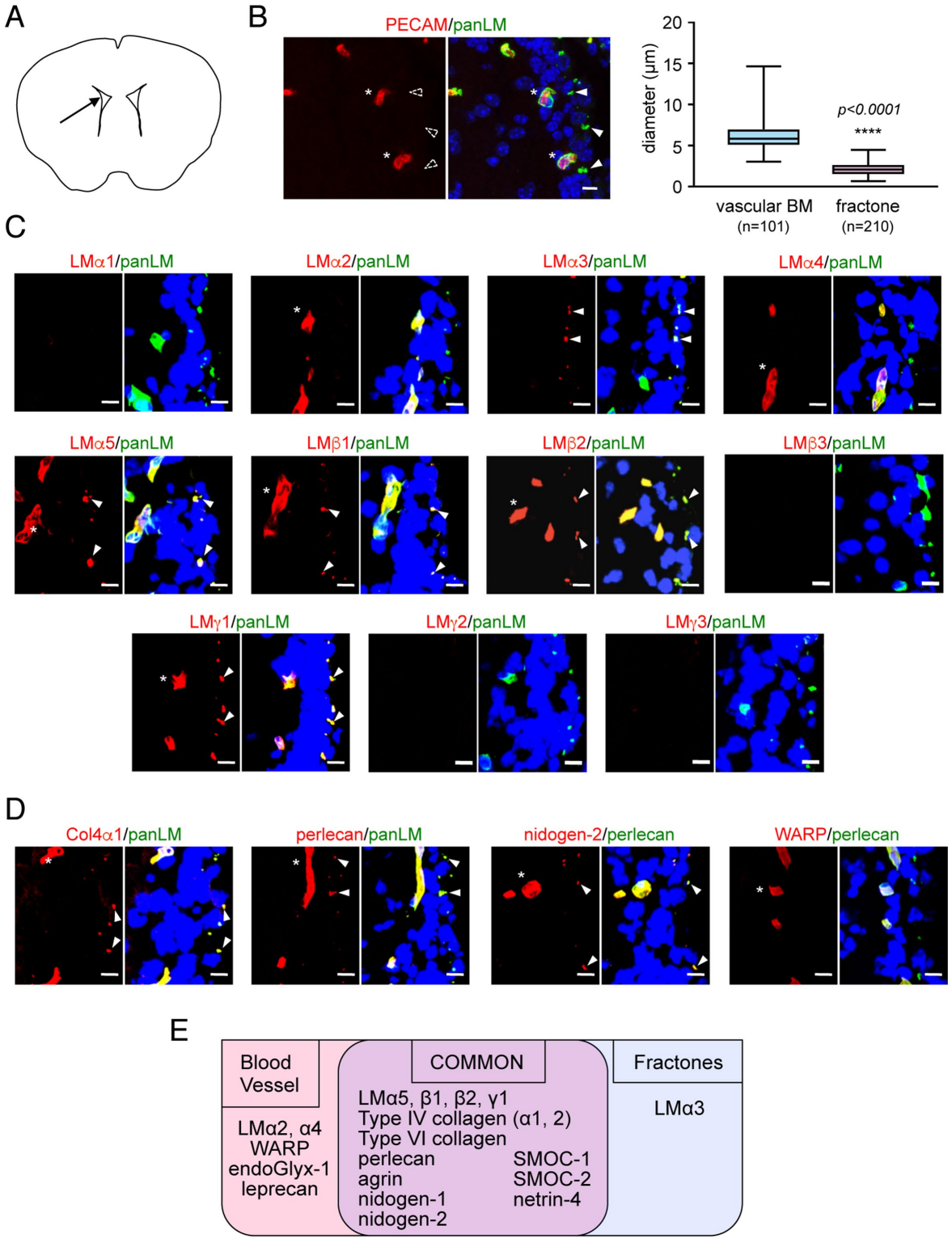

FIGURE 1: Molecular profiling of BM proteins in the adult mouse V-SVZ. (A) Schematic diagram depicting the position (arrow) of the images shown in the figure panels. (B) Morphological differences between vascular BMs and fractones. Left, vascular BMs are immunoreactive for both anti-panLM (green) and anti-PECAM (red) antibodies, while fractones are negative for the anti-PECAM antibody. Nuclei were stained with TO-PRO-3 (blue). Asterisks, vascular BMs; closed arrowheads, fractones; open arrowheads, fractones negative for the anti-PECAM antibody. Scale bar, 10 μm. Right, box-and-whisker plot showing the distributions of diameters for vascular BMs and fractones. (C, D) Immunohistochemical localization of individual LM subunits (C, red) and representative BM proteins (D, red) in the adult mouse V-SVZ. Anti-panLM or anti-perlecan antibodies (green) were used as BM markers. Nuclei were stained with Hoechst 33342 (blue). Asterisks, vascular BMs; arrowheads, fractones. Scale bars, 10 μm. (E) Summary of the BM protein profiles in the V-SVZ. See also Supplemental Figure S1.

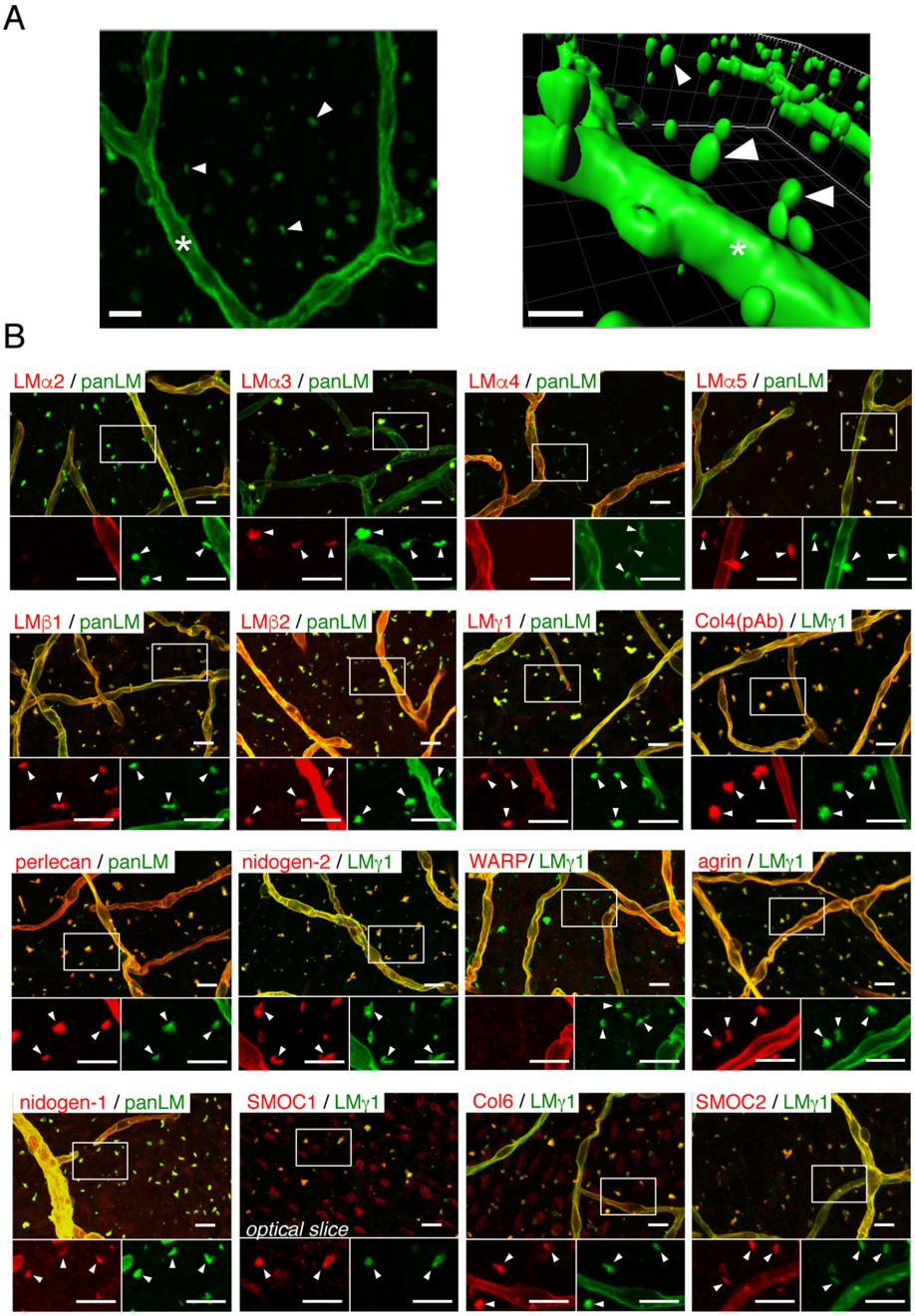

FIGURE 2: Fractones are visible as BM speckles in whole-mount V-SVZ immunostaining. (A) Whole-mount images of a mouse V-SVZ stained with an anti-panLM antibody. Left, image from the ventricle. Right, three-dimensional reconstruction of the left panel. See also Supplemental Movie S1. (B) Whole-mount V-SVZs were labeled with antibodies against individual BM proteins (red) together with anti-panLM or anti-LMγ1 antibodies (green). Each panel shows a merged image (top) and higher-magnification images (bottom) of the two channels in the boxed area. Asterisks, blood vessel BMs; arrowheads, speckled BMs. Scale bars, 10 μm.

Speckled BMs are produced at postnatal days 5–10

We investigated the timing of speckled BM production in the V-SVZ. Because speckled BMs were not observed in the V-SVZ of embryonic day 16.5 mice (Manabe *et al.*, 2008), we performed whole-mount V-SVZ immunostaining of mice from postnatal day 0 (P0) to P21 (Figure 3A). We also labeled V-SVZs with anti-β-catenin and anti-GFAP antibodies to visualize ependymal cell–cell junctions and adult NSCs/astrocytes, respectively. Speckled BMs were not detected at P0 and P3, but became apparent at P5 (Figure 3A and unpublished data), when ventricle-contacting cells differentiated into mature ependymal cells distinguishable by their large area of contact with the ventricles. Speckled BMs were more clearly observed at P7–P10, when mature ependymal cells and a small fraction of GFAP-positive NSCs/astrocytes emerged in the V-SVZ. At P14 and P21, the speckled BMs in the V-SVZ were indistinguishable from those in adult mice (Figure 3A and unpublished data). These results indicate that speckled BMs are produced in the V-SVZ at P5–P10.

Speckled BMs are localized at ependymal junctions and serve as scaffolds for a variety of V-SVZ cells

We further investigated the localization of speckled BMs within the V-SVZ. For this, we performed whole-mount immunostaining of V-SVZs from 7-wk-old adult mice with anti-β-catenin (Figure 3B), anti-doublecortin (Dcx, a marker for neuroblasts; Figure 3C), and anti-GFAP (Figure 3D) antibodies. Co-immunostaining for β-catenin and panLM revealed that speckled BMs were localized close to β-catenin-immunoreactive signals (Figure 3B), suggesting that the speckled BMs were deposited at or close to ependymal cell–cell junctions. We found that ~90% of ependymal cells came into close contact with speckled BMs (Figure 3E). A small proportion of speckled BMs also came into contact with Dcx-positive neuroblasts, although a large number of neuroblasts appeared to have no contact with speckled BMs (Figure 3, C and E). Interestingly, speckled BMs were often associated with GFAP-positive processes (Figure 3D, arrowheads). Similarly to the case for ependymal cells, ~90% of apical type B cells (GFAP-positive cells in close proximity to the lateral ventricle) adhered to speckled BMs (Figure 3E). The V-SVZs from GFAP-EGFP reporter mice also showed a close association of GFAP-EGFP-positive cells with LMγ1-positive speckled BMs (Supplemental Figure S3), suggesting that speckled BMs may serve as scaffolds for NSCs. This possibility was further assessed by 5-ethynyl-29-deoxyuridine (EdU) incorporation-chase assays, in which slowly dividing adult NSCs were visualized by EdU retention in their nuclei (Figure 3F). EdU was injected intraperitoneally into P21 mice once a day for 1 wk and chased for 2 wk. A fraction of EdU-labeled cells located at the center of the pinwheel structure had long GFAP-positive processes that made contact with both speckled BMs and blood vessels, suggesting that adult NSCs adhere to speckled BMs. Taken together, these results indicate that speckled BMs may serve as scaffolds for a variety of V-SVZ-residing cells, including ependymal cells, neuroblasts, astrocytes, and adult NSCs.

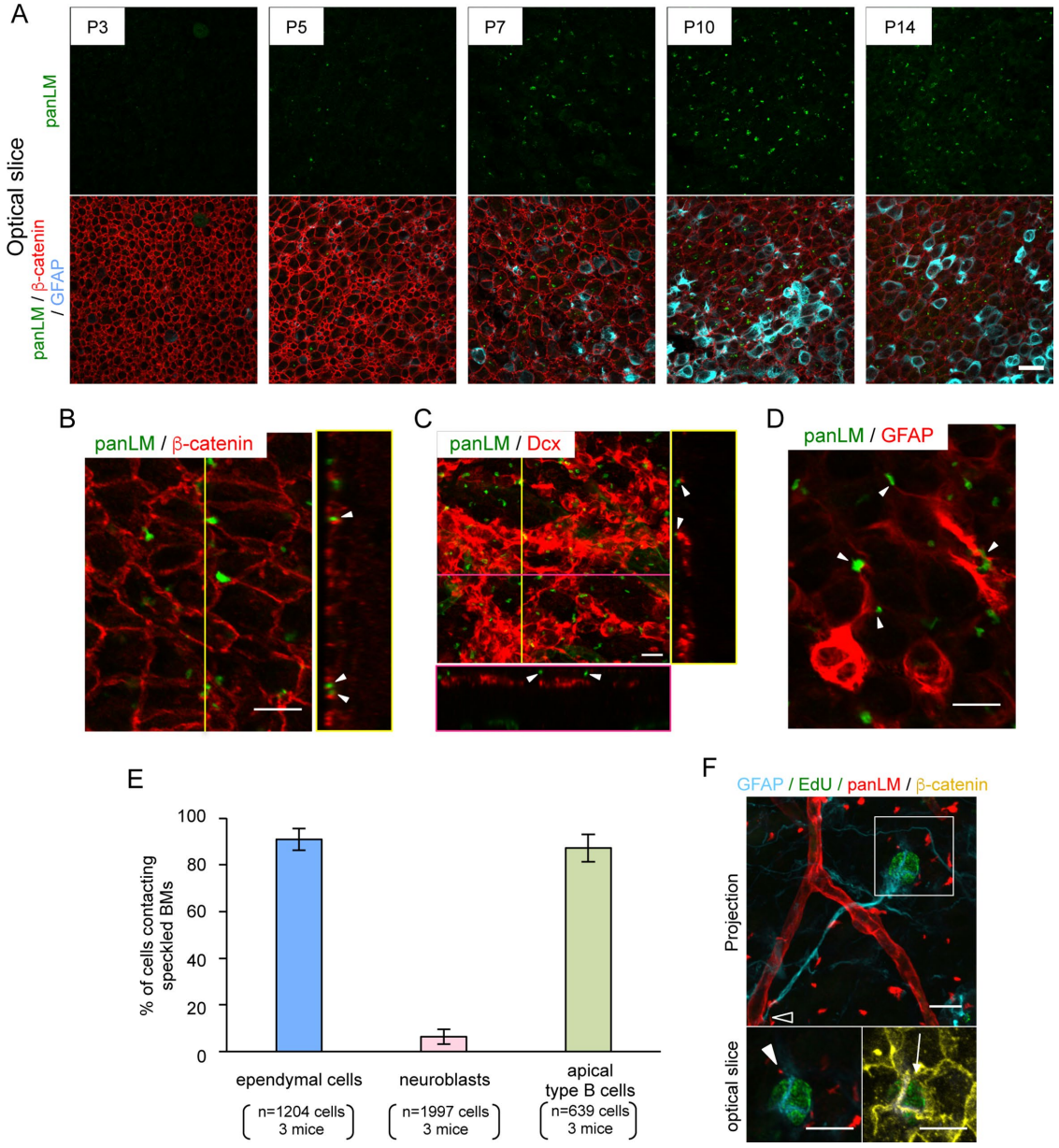

FIGURE 3: Speckled BMs are produced postnatally and localized between ependymal cells. (A) Time series observations of speckled BMs at the V-SVZ labeled with anti-panLM (green), anti-β-catenin (red), and anti-GFAP (cyan) antibodies. Images show superficial optical slices. Scale bar, 20 μm. (B–D) Representative images of V-SVZs colabeled with an anti-panLM antibody (green) and antibodies against (B) β-catenin (ependymal cell-cell junctions), (C) Dcx (neuroblasts), or (D) GFAP (NSCs/astrocytes). Orthogonal images at the yellow and/or magenta lines are shown in the right and bottom boxes, respectively (B, C). Speckled BMs (arrowheads) are located between ependymal cells and colocalized with GFAP-positive cells. See also Supplemental Figure S3. (E) Quantification of ependymal cells ($n = 1204$), neuroblasts ($n = 1997$), and apical type B cells ($n = 639$) adhering to speckled BMs. Randomly obtained images ($n = 8–10$) from three mice were analyzed. Error bars represent SD. (F) EdU was administered to P21 mice once a day for 1 wk and chased for 2 wk, followed by whole-mount V-SVZ staining to visualize label-retaining cells. Note that $GFAP^+/EdU^+$ cells adhere to blood vessels (open arrowhead) and speckled BMs (closed arrowhead) and have an apical process that makes contact with the ventricle (arrow). Scale bars, 10 μm.

GFAP-expressing cells, but not endothelial cells, produce LMα5 in speckled BMs

To elucidate the physiological roles of speckled BMs, it is necessary to determine which cells produce speckled BMs in the V-SVZ. To this end, we generated conditional *Lama5*-null mice (Figure 4A). First, we performed whole-mount immunostaining of V-SVZs from endothelium-specific *Lama5*-knockout mice (*Tie2-Cre;Lama5*$^{fl/fl}$) to visualize the LMα5 localization in vascular BMs and speckled BMs (Figure 4B). In control *Tie2-Cre;Lama5*$^{fl/+}$ mouse V-SVZs, LMα5 was detected in both vascular BMs and speckled BMs. In contrast, *Lama5*-knockout mouse V-SVZs showed severely impaired LMα5 expression in vascular BMs, confirming *Tie2-Cre*-mediated deletion of LMα5 in endothelial cells. However, the LMα5 deposition in speckled BMs was comparable to that in control mice, indicating

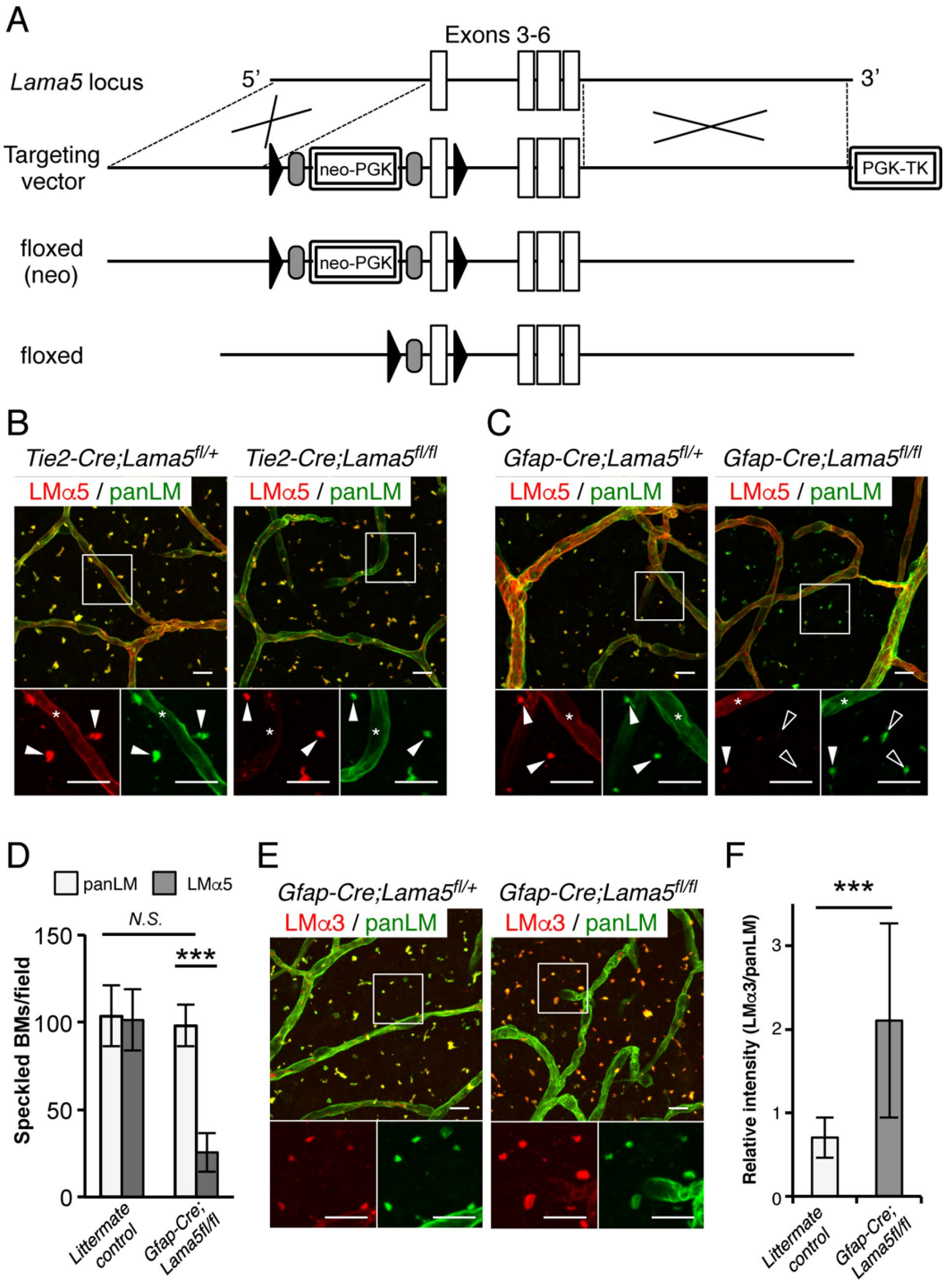

FIGURE 4: GFAP-positive NSCs produce speckled BMs. (A) Schematic diagrams of the wild-type *Lama5* allele, targeting vector, targeted floxed$^{(neo)}$ allele, and floxed allele. Cre-mediated recombination removes exon 3, resulting in a frame-shift error. Open boxes, exons; closed triangles, loxP sites; gray ovals, FRT sites. Whole-mount V-SVZs from *Tie2-Cre;Lama5$^{fl/fl}$* (B) and *Gfap-Cre;Lama5$^{fl/fl}$* (C) mice were labeled with anti-panLM (green) and anti-LMα5 (red) antibodies. Each panel shows a merged image (top) and higher-magnification images (bottom) of the two channels in the boxed area. Asterisks, vascular BMs; closed arrowheads, speckled BMs; open arrowheads, speckled BMs without LMα5 deposition. (D) Quantification of the speckled BMs positive for panLM or LMα5. Randomly obtained images from three control littermates ($n = 6$ images in total) and three *Gfap-Cre;Lama5$^{fl/fl}$* mice ($n = 7$ images in total) were analyzed. Data represent means ± SEM. ***$p < 0.001$. (E, F) Whole-mount V-SVZs from *Gfap-Cre;Lama5$^{fl/fl}$* mice were labeled with anti-panLM (green) and anti-LMα3 (red) antibodies. Each panel shows a merged image (top) and higher-magnification images (bottom) of the two channels in the boxed area. Note that immunoreactivity for LMα3 is up-regulated two- to threefold in *Gfap-Cre;Lama5$^{fl/fl}$* mice compared with control mice (F). ***$p < 0.001$. Scale bars, 10 μm.

that the α5-containing LMs in speckled BMs were not derived from endothelial cells.

Given the close proximity of GFAP-positive cells to speckled BMs (Figure 3D), we examined the possibility that GFAP-positive cells produce speckled BMs. V-SVZs from transgenic mice specifically lacking *Lama5* in GFAP-positive NSCs/astrocytes (*Gfap-Cre;Lama5*$^{fl/fl}$) were immunostained with an anti-LMα5 antibody (Figure 4C). In comparison with V-SVZs from control *Gfap-Cre;Lama5*$^{fl/+}$ mice, the LMα5 immunoreactivity was significantly compromised in speckled BMs, but not vascular BMs, in *Gfap-Cre;Lama5*$^{fl/fl}$ mice. Quantification revealed that ~80% of speckled BMs were negative for LMα5 in *Gfap-Cre;Lama5*$^{fl/fl}$ V-SVZs, although the total number of speckled BMs remained unchanged (Figure 4D). These results indicate that the LMα5 in speckled BMs mainly originates from GFAP-expressing cells, suggesting that speckled BMs are deposited by NSCs/astrocytes.

The speckled BMs in *Gfap-Cre;Lama5*$^{fl/fl}$ mice also exhibited up-regulation of LMα3 (Figure 4, E and F), whose receptor-binding profiles overlap with those of α5-containing LMs (Nishiuchi *et al.*, 2006). These results indicate compensation by LMα3 for loss of LMα5 in speckled BMs.

Speckled BMs bind to integrins

Given the up-regulation of LMα3 in *Gfap-Cre;Lama5*$^{fl/fl}$ mice, we hypothesized that speckled BMs function as cell-adhesive scaffolds for cells residing in the V-SVZ. To explore this possibility, we examined the integrin-binding activities of speckled BMs by in situ integrin overlay assays. For these experiments, the distribution of a wide range of integrin ligands was visualized in frozen tissue sections by incubation with recombinant soluble integrins in the presence of Mn^{2+} (Kiyozumi *et al.*, 2012, 2014; Sato-Nishiuchi *et al.*, 2012). Among the LM-binding integrins examined, α3β1, α6β1, and α7X1β1 integrins were capable of binding to speckled BMs in situ (Figure 5A). The speckled BMs failed to bind to α7X2β1 integrin, a receptor for α1- and α2-containing LMs (Nishiuchi *et al.*, 2006), consistent with the absence of these LMs in speckled BMs. In addition, the collagen-binding integrins α1β1 and α2β1 and the Arg–Gly–Asp (RGD) motif-binding integrin αVβ5 bound to speckled BMs (Supplemental Figure S4). No signals were detected when integrins were overlaid in the presence of 10 mM EDTA, confirming the specificity of the in situ integrin-binding assays (Figure 5A and Supplemental Figure S3, right). These results demonstrate that speckled BMs harbor various integrin ligands and raise the possibility that cells residing in the V-SVZ adhere to speckled BMs via integrins. Consistent with this possibility, the majority of speckled BMs were immunoreactive for α6 integrin (Figure 5B), an LM-binding integrin expressed in neural stem/progenitor cells (Shen *et al.*, 2008; Kazanis *et al.*, 2010). These results suggest that α6 integrin mediates cell adhesion to speckled BMs.

Perturbation of LM integrin-binding activity impairs speckled BM formation

To investigate the physiological role of the interactions of speckled BMs with integrins, we employed conditional transgenic mice expressing an E1605Q mutant of LMγ1 (Figure 6, A and B). The E1605 residue is located at the third position from the C-terminus in the mouse LMγ1 chain (Figure 6A) and the E1605Q substitution abolishes LM binding to integrins (Ido *et al.*, 2007). The integrin-binding activities of speckled BMs in *Gfap-Cre;Lamc1*$^{cEQ/cEQ}$ mice were examined by in situ integrin-binding assays (Figure 6C). We used α3β1 integrin as a probe because of its specific detection of speckled BMs containing α3/5-LMs (Figure 5A) (Nishiuchi *et al.*, 2006). In

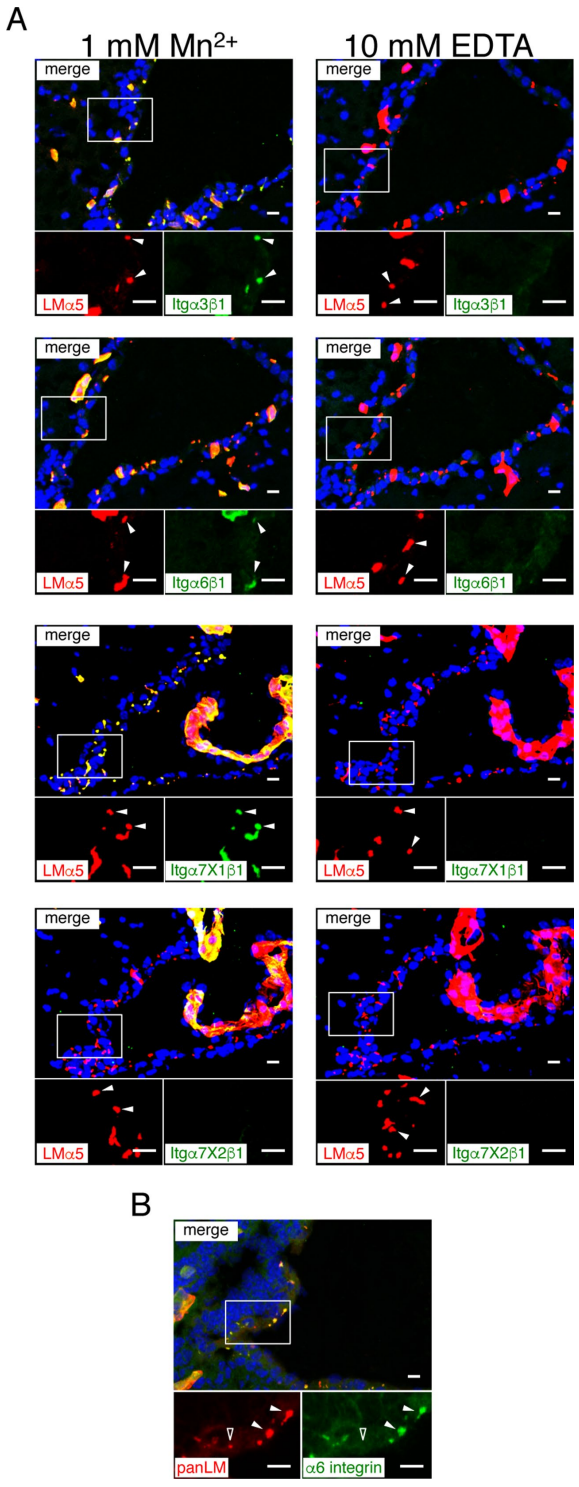

FIGURE 5: Integrin-binding activity of speckled BMs. (A) Cryosections of adult mouse brains were incubated with recombinant integrins (green) in the presence of 1 mM $MnCl_2$ (left) or 10 mM EDTA (right). An anti-LMα5 (red) antibody was used as a marker for speckled and vascular BMs. Nuclei were stained with Hoechst 33342 (blue). Each panel shows a merged image (top) and higher magnification images (bottom) of the two channels in the boxed area. Arrowheads, speckled BMs. See also Supplemental Figure S4. (B) Cryosections of adult mouse brains were labeled with anti-α6 integrin (green) and anti-panLM (red) antibodies. Closed and open arrowheads indicate speckled BMs positive and negative for α6 integrin, respectively. Scale bars, 10 μm.

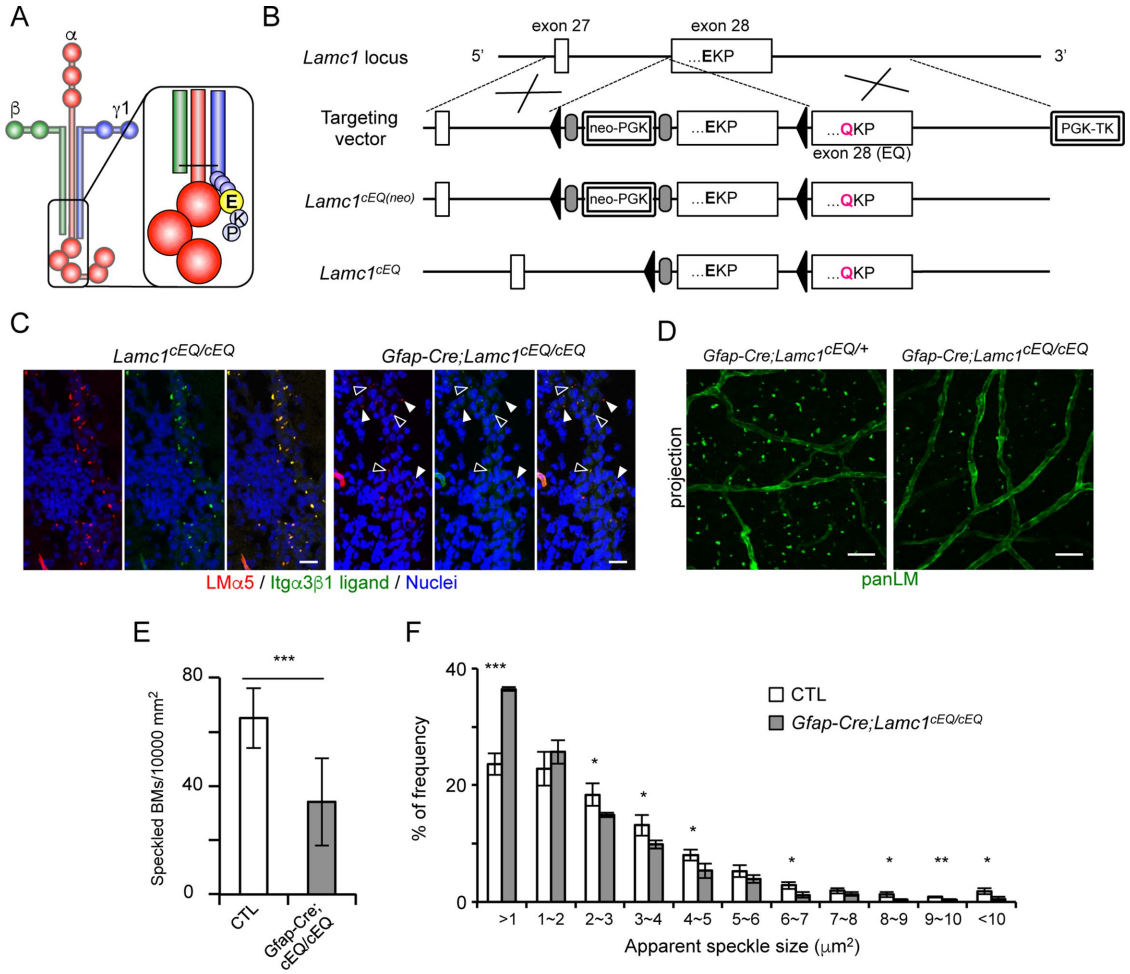

FIGURE 6: Disruption of LM integrin-binding activity causes impaired formation of speckled BMs. (A) Schematic model of a γ1-containing LM. The Glu (E) residue at the third position from the C-terminus of LMγ1 (highlighted by a yellow sphere in the inset) is a prerequisite for interactions with integrins. (B) Schematic diagrams of the wild-type *Lamc1* allele, targeting vector, targeted floxed$^{cEQ(neo)}$ allele, and floxed^{cEQ} allele. Cre-mediated recombination removes the wild-type exon 28, resulting in transcription of exon 28 (EQ). Open boxes, exons; closed triangles, loxP sites; gray ovals, FRT sites. (C) Cryosections of adult brains from *Gfap-Cre;Lamc1*$^{cEQ/cEQ}$ mice were probed with α3β1 integrin (green) in the presence of 1 mM $MnCl_2$. An anti-LMα5 (red) antibody was used as a marker for speckled BMs. Nuclei were stained with Hoechst 33342 (blue). Open and closed arrowheads indicate speckled BMs with and without bound α3β1 integrin, respectively. Scale bars, 10 μm. (D) Whole-mount V-SVZs from *Gfap-Cre;Lamc1*$^{cEQ/cEQ}$ mice were labeled with an anti-panLM antibody. Scale bars, 20 μm. Quantification of speckled BMs (E) and histogram of speckled BM areas (F). Data represent means ± SEM in 20 and 15 randomly obtained images from four control (CTL) and three *Gfap-Cre;Lamc1*$^{cEQ/cEQ}$ mice, respectively. *$p < 0.05$; **$p < 0.01$; ***$p < 0.001$.

control *Lamc1*$^{cEQ/cEQ}$ mice, almost all speckled BMs were capable of binding to α3β1 integrin. In *Gfap-Cre;Lamc1*$^{cEQ/cEQ}$ mice, speckled BMs were fewer and less prominent, and about half of the speckled BMs were devoid of α3β1 integrin binding, suggesting that E1605Q-containing LMs accumulated in the speckled BMs. Whole-mount V-SVZ immunostaining (Figure 6D) further revealed a 50% reduction in the number of speckled BMs (Figure 6E) and a significant increase in small (<1 μm^2) speckles (Figure 6F) in comparison with control mice. These results indicate that interactions between LMs and integrins are required for proper assembly of speckled BMs in the V-SVZ.

Impaired formation of speckled BMs causes reduced NSC proliferation in vitro

To further explore the functions of speckled BMs as an NSC niche, we investigated the NSC phenotypes in the V-SVZ of *Gfap-Cre;Lamc1*$^{cEQ/cEQ}$ mice. Because speckled BM formation was significantly impaired in the *Gfap-Cre;Lamc1*$^{cEQ/cEQ}$ mouse V-SVZ (Figure 6, D–F), we hypothesized that NSC adhesion to speckled BMs is compromised in *Gfap-Cre;Lamc1*$^{cEQ/cEQ}$ mice. To confirm this possibility, whole-mount V-SVZs from *Gfap-Cre;Lamc1*$^{cEQ/cEQ}$ mice were coimmunostained with anti-panLM and anti-GFAP antibodies to visualize the positional correlation between speckled BMs and NSCs. While ~80% of NSCs, defined as GFAP-positive cells in close proximity to the lateral ventricle (so-called apical B cells), came into contact with speckled BMs in the control mouse V-SVZ, only 50% of NSCs were associated with speckled BMs in the *Gfap-Cre;Lamc1*$^{cEQ/cEQ}$ mouse V-SVZ (Figure 7, A and B), without affecting the number of apical B cells (Figure 7C). Given the reduced integrin-binding activity of speckled BMs in the mutant mice, these results suggest that NSCs are more likely to become detached from speckled BMs. In addition, NSCs in the *Gfap-Cre;Lamc1*$^{cEQ/cEQ}$ mouse V-SVZ exhibited higher GFAP expression than those in the control

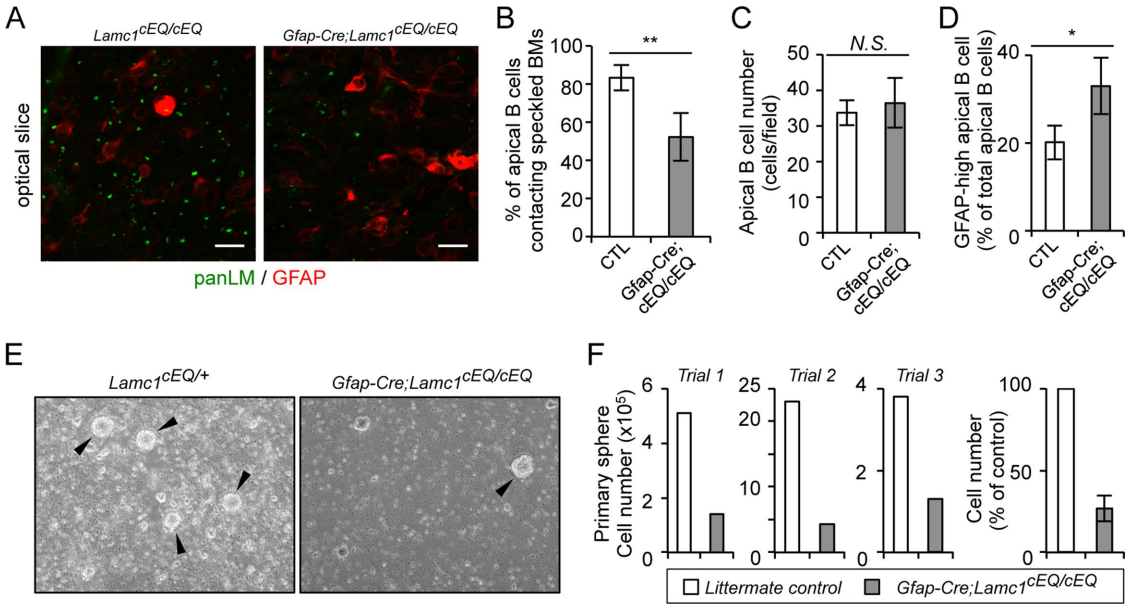

FIGURE 7: NSCs from conditional *Lamc1* mutant mice exhibit reduced proliferation in vitro. (A) Whole-mount V-SVZs from *Gfap-Cre;Lamc1*$^{cEQ/cEQ}$ mice were labeled with anti-panLM (green) and anti-GFAP (red) antibodies. Data show superficial optical slices at the ependymal cell layer. Scale bars, 10 μm. Numbers of apical B cells making contact with speckled BMs (B), total numbers of apical B cells (C), and numbers of GFAP-high apical B cells exhibiting saturated GFAP signals (D). Data represent means ± SEM of cell numbers in 20 and 15 randomly obtained images from four control littermates (CTL) and three *Gfap-Cre;Lamc1*$^{cEQ/cEQ}$ mice, respectively. (E) Representative images of primary neurospheres generated from *Gfap-Cre;Lamc1*$^{cEQ/cEQ}$ and control *Lamc1*$^{cEQ/+}$ mice. Arrowheads indicate neurospheres. (F) Quantification of cells plated at a density of 4000 cells/cm^2 with EGF and basic FGF under nonadherent conditions and cultured for 7 d. Data represent means ± SD of three independent examinations. *$p < 0.05$; **$p < 0.01$.

mouse V-SVZ (Figure 7D), suggesting that the integrin signals suppress GFAP expression, as previously described (Robel *et al.*, 2009). Ependymal cells in the *Gfap-Cre;Lamc1*$^{cEQ/cEQ}$ mouse V-SVZ formed tight junctions, ependymal cilia, and a pinwheel-like organization resembling those in control mice (Figure S5), suggesting that inactivation of speckled BMs did not affect the apicobasal polarity of ependymal cells.

Next, we examined whether the proliferative potential of NSCs was affected in *Gfap-Cre;Lamc1*$^{cEQ/cEQ}$ mice. When V-SVZ cells from control mice were cultured in vitro, NSCs proliferated as neurospheres (Figure 7E), yielding a 4- to 20-fold increase in the total cell number in the first 7 d (Figure 7F). In contrast, V-SVZ cells from *Gfap-Cre;Lamc1*$^{cEQ/cEQ}$ mice rarely gave rise to neurospheres, resulting in a 70% reduction in the cell number after 7 d in vitro in comparison with control mice (Figure 7, E and F). The sphere-forming efficiency of V-SVZ cells from *Gfap-Cre;Lamc1*$^{wild/wild}$ mice was comparable to that of cells from wild-type mice (unpublished data), indicating that the Cre expression in NSCs did not affect the generation of neurospheres. These results suggest that the Gfap-Cre-mediated LMγ1 E1605Q knockin causes NSC detachment from speckled BMs and reduces their potential to form neurospheres, consistent with the possibility that speckled BMs may serve as a niche for NSCs to regulate their behaviors.

DISCUSSION

One of the fundamental goals of stem cell research is to elucidate the molecular mechanisms by which inherent in vivo niche factors affect stem cell physiology. Although BMs are considered to serve as a niche for various tissue stem cells, the detailed molecular compositions and functions of BMs composing the stem cell niche are poorly understood. In the present study, we used immunohistochemistry to generate a comprehensive list of BM proteins localized at vascular BMs and fractones/speckled BMs. Speckled BMs are mainly derived from GFAP-expressing cells and make direct contact with NSCs. Loss of function of speckled BMs results in impaired NSC proliferation. Our results indicate that speckled BMs provide adhesive substrates for NSCs and regulate NSC proliferation.

The molecular compositions of BMs vary among tissues (Manabe *et al.*, 2008). This diversity in protein compositions confers a wide array of receptor-binding properties on individual BMs. Among BM proteins, LMα chains are representative because they display clear tissue-specific distribution patterns: LMα1 is mainly localized at Reichert's membrane, while LMα2 and LMα4 are present in muscular and vascular BMs, respectively (Aumailley, 2013). In this regard, the LMα chain composition of fractones/speckled BMs is intriguing, because they are composed of LMα3 and LMα5, which are typically expressed in BMs underlying cells of ectodermal origin, including NSCs and epidermal cells (Miner *et al.*, 1997; Li *et al.*, 2003). The NSC adhesion to α3/5-containing LMs underscores the importance of integrin signaling, because both types of LMs exhibit strong binding toward α3β1 and α6β1 integrins (Nishiuchi *et al.*, 2006), with the latter being expressed in NSCs (Shen *et al.*, 2008). Given the similar integrin-binding properties of α3/5-containing LMs and the expression of α6β1 integrin in NSCs, our observations suggest that α6β1 integrin signaling is involved in the regulation of NSC proliferation. Indeed, several lines of evidence suggest that α6β1 integrin, which colocalizes with fractones/speckled BMs, affects NSC proliferation through mitogen-activated protein kinase (MAPK) pathways (Staquicini *et al.*, 2009). Alternatively, α6β1 integrin may alter the localization of BMP receptors on NSCs and thereby modulate BMP signaling (North *et al.*, 2015).

Our whole-mount V-SVZ immunostaining and molecular profiling of BM proteins demonstrated that the speckled BMs in the V-SVZ are equivalent to the fractones observed in tissue sections. Although BM speckles in the V-SVZ were found in previous whole-mount studies (Shen *et al.*, 2008; Codega *et al.*, 2014), it remained controversial whether these speckles were fractones. Shen *et al.* (2008) argued that the BM speckles were part of the endothelial BMs, while Codega *et al.* (2014) assigned them as fractones. This controversy may have arisen through the limited probes available for BM proteins and the ambiguity in fractone structures. Although Mercier *et al.* (2002) proposed that fractones are fingerlike fibrous processes of extravascular BMs called "stems," and terminate at the ependymal layer to form large "bulbs," our results suggest that fractones are speckled BMs and independent of the vasculature. First, fibrous BM structures corresponding to the "stems" of fractones were hardly detected in whole-mount observations. Because Mercier *et al.* (2002) described that Formalin fixation was detrimental for fractone visualization, we examined the speckled BMs by whole-mount immunostaining with several fixatives, including Formalin, methanol, and/or acetone, with or without perfusion fixation by paraformaldehyde. We found that speckled BMs, rather than fibrous BMs extending from vascular BMs, were reproducibly observed under all conditions, showing only differences in signal intensity (unpublished data). Fibrous BMs were visible around large blood vessels (Supplemental Figure S2). Second, speckled BMs were sparsely, but ubiquitously, distributed throughout the V-SVZ surface, irrespective of vascular and avascular areas (Figure 2A). If fractones were extended from vascular BMs, the V-SVZ in vascular areas would be enriched in fractones. Third, GFAP-positive cells, possibly NSCs but not endothelial cells, produced and adhered to fractones/speckled BMs. The production of punctate BMs was previously observed with astrocytes and NSCs (Liesi and Silver, 1988; Milner, 2007).

BMs are assembled by multiple interactions of BM proteins, among which LMs are important because their loss prevents BM formation and leads to early embryonic lethality (Smyth *et al.*, 1999; Miner *et al.*, 2004). The assembly of LMs, typically α1/2-containing LMs, occurs at the cell surface and requires interactions of LMs with receptors and/or sulfated glycosides/glycolipids, in other words, integrins, dystroglycan, and heparan sulfate/sulfatide (Yurchenco *et al.*, 2004). In this study, we have shown a critical role of LM–integrin interactions in the assembly of speckled BMs. Recently, McClenahan *et al.* (2016) revealed a role of dystroglycan in accumulation of LM-rich "hubs," equivalent to the speckled BMs, in the adult mouse V-SVZ. Although the apparent structure of speckled BMs is completely different from that of typical sheetlike BMs, these results indicate the involvement of the two major LM receptors, integrins and dystroglycan, in speckled BM assembly. Thus, a similar, if not identical, mechanism seems to operate in the formation of speckled BMs and sheet-like BMs. The hypomorphic speckled BMs in *Gfap-Cre;Lamc1*$^{cEQ/cEQ}$ mice may arise through partial compensation by dystroglycan in speckled BM assembly. It should be noted that, in contrast to α1/2-containing LMs, whose dystroglycan-binding domains are relatively resistant to proteolysis, α3/5-containing LMs are known to be sensitive to proteolysis, resulting in the removal of their dystroglycan/heparan sulfate-binding domains (Ido *et al.*, 2004; Rousselle and Beck, 2013). Although it remains unclear whether the dystroglycan-binding domains of α3/5-containing LMs are retained in speckled BMs, a previous study showed a dotlike distribution of β-dystroglycan in the V-SVZ, reminiscent of the speckled BMs/fractones (Adorjan and Kalman, 2009). It is an intriguing question how dystroglycan and integrins cooperate in the assembly of α3/5-containing LMs in speckled BMs.

Although adult NSCs have characteristics of embryonic radial glial cells, such as contact with the ventricle and possession of a primary cilium (Kriegstein and Alvarez-Buylla, 2009), it remains uncertain whether the niche for adult NSCs is similar to, or different from, that for embryonic radial glial cells. Radial glial cells can divide rapidly and give rise to the vast majority of neurons, astrocytes, ependymal cells, and oligodendrocytes, while adult NSCs rarely proliferate and give rise to olfactory interneurons in a homeostatic state (Kriegstein and Alvarez-Buylla, 2009). In this study, we have demonstrated that speckled BMs/fractones first appear at P5, when ventricle-contacting radial glial cells change their morphology and differentiate into mature ependymal cells and adult NSCs (Merkle *et al.*, 2004). The coemergence of speckled BMs with maturation of ependymal cells and adult NSCs is indicative of a role for speckled BMs in the adult, but not the embryonic, NSC niche. As infrequent proliferation is intrinsic to adult NSCs, it is tempting to speculate that speckled BMs may serve as adhesive substrates for NSCs to retain them in a neurogenic niche, because speckled BMs/fractones have been shown to entrap a variety of neurogenesis-stimulating molecules in the CSF (Kerever *et al.*, 2007; Douet *et al.*, 2013). The enlargement of speckled BMs/fractones in aged rodents (Kerever *et al.*, 2015) may reflect a potential role of speckled BMs in neurogenic signaling, because aged NSCs may require strong stimuli to undergo proliferation.

Adult NSCs are tightly sandwiched between the lateral ventricle wall and the vascular plexus (Bjornsson *et al.*, 2015). The cellular architecture of the adult NSC niche in the V-SVZ suggests two areas of the NSC niche, ependymal/CSF niche and vascular niche (Kokovay *et al.*, 2010), the former of which is enriched in signaling molecules for NSC proliferation and neurogenesis. For example, TGF-α (EGF receptor ligand) and basic FGF, which are both required for NSC proliferation (Rietze and Reynolds, 2006), are expressed in the choroid plexus, which is responsible for continuously producing the bulk of the CSF (Bjornsson *et al.*, 2015). Ependymal cells have been shown to express noggin, an inhibitor of BMPs that negatively impact neurogenesis (Lim *et al.*, 2000; Douet *et al.*, 2012), and the chemoattractant CXCL12/SDF-1 (Kokovay *et al.*, 2010), thereby having the potential to promote NSC proliferation and retain NSCs in the neurogenic niche. The proliferative activity of NSCs was found to be correlated with distance from ependymal cells within 5 μm from the lateral ventricle, but unrelated to distance from the vasculature (Kazanis *et al.*, 2010). However, a recent study revealed that vascular endothelial cells provide NSCs with a quiescent niche, because direct contact of NSCs with vascular endothelial cells, together with endothelium-derived soluble factors, suppressed NSC proliferation while maintaining the stem cell identity (Ottone *et al.*, 2014; Sato *et al.*, 2017). These observations suggest that ependymal/CSF-derived factors activate the proliferation and neurogenesis of NSCs, while interaction with the vasculature produces dormant signals for NSCs. Given that speckled BMs are localized between/beneath ependymal cells and make contact with NSCs, speckled BMs may function as a substrate for NSCs to adhere to the ependymal/CSF niche, thereby providing them with activating signals from the niche. Disruption of the interactions between NSCs and speckled BMs by the *Lamc1*^{E1605Q} mutation may perturb the activation signals for NSCs from the ependymal/CSF niche, resulting in a quiescence-dominant state of NSCs. In support of this scenario, impaired neurosphere formation and higher GFAP expression were observed in V-SVZ cells from *Gfap-Cre;Lamc1*$^{cEQ/cEQ}$ mice. Accumulating evidence indicates that quiescent NSCs rarely give rise to neurospheres and exhibit higher GFAP expression than active NSCs (Codega *et al.*, 2014; Llorens-Bobadilla *et al.*, 2015) Alternatively,

integrin-dependent adhesion signals may influence the proliferation of NSCs, as shown in a previous study (Jacques *et al.*, 1998).

During the preparation of this manuscript, Nascimento *et al.* (2018) reported an excellent study providing insights into the structure, origin, and physiological function of fractones as an NSC niche, which are basically consistent with our observations. However, there are some conflicts between our observations and their findings. They showed that LMα2 is deposited on fractone stems, fibrous BM structures extended from vascular BMs, while we were unable to detect LMα2 in fractone stems because fibrous BM structures were hardly observed in our whole-mount V-SVZ immunostaining. In contrast, our observations clearly showed that speckled BMs contain LMα3, while Nascimento *et al.* (2018) were unable to detect LMα3 in fractone bulbs. These discrepancies may arise through differences in the antibody epitopes or ages of mice analyzed. In addition, Nascimento *et al.* (2018) used the *FoxJ1-Cre* line and demonstrated that fractones originate from ependymal cells, while we identified NSCs/astrocytes as the producers of speckled BMs. It should be noted that a small subpopulation of ventricle- and blood vessel-contacting astrocytes, possibly apical type B1 cells, has been shown to express FoxJ1 (Jacquet *et al.*, 2009). Therefore, use of the *FoxJ1-Cre* line cannot exclude the possibility that NSCs produce speckled BMs/fractones. Given that neither ependymal cell- nor NSC/astrocyte-specific Cre lines exhibited complete loss of LMα5 in speckled BMs, these results strongly suggest that both ependymal cells and NSCs produce speckled BMs in the V-SVZ, leading to the hypothesis that speckled BM production is a common feature of ventricle-contacting cells. It is an intriguing issue for further investigation to establish whether combinations of *FoxJ1-Cre* and *Gfap-Cre* lines can result in complete loss of speckled BMs.

In conclusion, we have shown that speckled BMs/fractones are deposited by GFAP-expressing cells through their interactions with integrins and serve as adhesive substrates for NSCs. Although the physiological roles of speckled BMs/fractones require further examination in vivo, our results show that adhesion of NSCs to speckled BMs/fractones may regulate NSC proliferation as part of the stem cell niche. Further studies on the roles of ECMs/BMs will provide insights into how NSCs are regulated in their in vivo niche and how these cells can be expanded ex vivo for application in regenerative medicine.

MATERIALS AND METHODS

Animals

To generate the floxed *Lama5* and *Lamc1*^{E1605Q} (designated *Lamc-1*^{cEQ}) alleles, genomic DNA fragments containing exons 3–6 of *Lama5* and exons 27 and 28 of *Lamc1* were used for gene targeting. A loxP-FRT-PGK-neo-FRT cassette was inserted, as shown in Figures 4A and 6A. The linearized targeting vectors were transfected into embryonic stem cells, and several homologous recombinants were identified by PCR. Independent clones that retained the loxP site were injected into C57Bl/6 blastocysts to generate germline chimeras. The chimeras were bred with mice expressing FLPe recombinase to remove the selective marker and generate the conditional *Lama5*^{fl} and *Lamc1*^{cEQ} alleles. *Lama5*$^{fl/fl}$ and *Lamc1*$^{cEQ/cEQ}$ mice were maintained on a C57Bl/6 × 129/Sv mixed background and were indistinguishable from littermates carrying wild-type *Lama5* and *Lamc1* alleles, respectively.

Tie2-Cre (Jackson Laboratory; #008863) and Gfap-Cre (Jackson Laboratory; #012886) transgenic mice were bred with mice possessing *Lama5*^{fl} and *Lamc1*^{cEQ} alleles to generate *Tie2-Cre;Lama5*$^{fl/fl}$, *Gfap-Cre;Lama5*$^{fl/fl}$, and *Gfap-Cre;Lamc1*$^{cEQ/cEQ}$ mice. GFAP-EGFP transgenic mice were obtained from Jackson Laboratory (#010835). C57Bl/6J and ICR mice were purchased from Japan SLC (Hamamatsu, Japan). All mouse experiments were performed in compliance with our institutional guidelines and were approved by the Animal Care Committee of Osaka University.

Antibodies and reagents

Freestyle 293-F cells were obtained from Life Technologies (Gaithersburg, MD). The primary antibodies used for immunohistochemical analyses are listed in Supplemental Table S1. All of the BM antibodies raised in our laboratory were described in our previous paper (Manabe *et al.*, 2008) and the Mouse Basement Membrane Bodymap database (http://dbarchive.biosciencedbc.jp/archive/matrixome/bm/home.html). We validated the specificities of the antibodies using the following criteria, with all of the antibodies meeting criteria #1 and #2 and at least one of criteria #3, #4, and #5:

1. Specific recognition of the antigenic fragment in enzyme-linked immunosorbent assay (ELISA) and Western blotting
2. Specific recognition of the full-length recombinant protein expressed in mammalian cells in ELISA and Western blotting
3. Loss of immunohistochemical reactivity upon adsorption with the antigenic fragment and full-length recombinant protein
4. Production of a staining pattern identical to that of corresponding antibodies raised against nonoverlapping fragments
5. Immunohistochemical staining pattern similar to that published in the literature.

Alexa Fluor-conjugated secondary antibodies were obtained from Life Technologies. Hoechst 33342 and TO-PRO-3 were purchased from Thermo Fisher Scientific (Waltham, MA). Normal goat serum was purchased from Vector Laboratories (Burlingame, CA).

Immunohistochemistry of brain sections

Brains from adult mice (7 wk of age) were embedded in OCT compound for cryosectioning. The obtained sections (8–10-μm thickness) were fixed with 3.7% formaldehyde (staining for PECAM, nidogen-1, and LMα4) or 100% acetone at −30°C (staining for other proteins), blocked with phosphate-buffered saline (PBS) containing 10 mg/ml bovine serum albumin (BSA), and probed with primary and Alexa Fluor-conjugated secondary antibodies. The sections were counterstained with Hoechst 33342, mounted with FluorSave reagent (Calbiochem, San Diego, CA), and visualized using an LSM5 (Carl Zeiss, Oberkochen, Germany) or TCS SP5 (Leica, Wetzlar, Germany) laser scanning microscope.

Whole-mount immunostaining of V-SVZ

V-SVZ whole mounts of the striatal lateral wall were dissected from 7- to 15-wk-old C57Bl/6J or P0–P21 ICR mice as described (Tavazoie *et al.*, 2008). The whole mounts were fixed in 100% methanol, washed with PBS containing 0.1% Triton X-100, and blocked with PBS containing 10% normal goat serum and 1% Triton X-100 (blocking buffer). The samples were then incubated with primary antibodies for 3–4 d, followed by secondary antibodies for 2–3 d. After washing, the samples were dehydrated in a graded methanol series (50, 80, and 100%) and sequentially immersed in a 1:2:3 mixture of benzyl alcohol (Sigma, St. Louis, MO; 402834), benzyl benzoate (Sigma; B6630), and methanol and a 1:2 mixture of benzyl alcohol and benzyl benzoate. Finally, the samples were mounted on glass slides with a Secure-Seal spacer (Life Technologies) and visualized using an LSM5, TCS SP5, or FV1200 (Olympus, Tokyo, Japan) laser scanning microscope. Each set of stained samples was processed under identical gain and laser power settings. Three-dimensional

reconstruction and surface rendering were performed with Imaris version 7.6.4 image analysis software (Bitplane, Zurich, Switzerland). The number and size of speckled BMs were measured by ImageJ version 2.0 software (Schneider *et al.*, 2012). GFAP-expressing apical B cells that exhibited saturated GFAP signals were defined as GFAP-high cells and manually counted.

Purification of recombinant integrins and in situ integrin-binding assay

Purification of recombinant integrins and in situ integrin-binding assays were performed as described previously (Nishiuchi *et al.*, 2006; Kiyozumi *et al.*, 2012, 2014). Frozen sections of adult mouse brains were fixed with 100% acetone, blocked, and incubated with recombinant integrins in the presence of 1 mM Mn^{2+}. Negative control sections were incubated with recombinant integrins in the presence of 10 mM EDTA. After being washed with Tris-buffered saline containing 1 mM Mn^{2+}, the sections were incubated with a rabbit anti-"Velcro" (ACID/BASE coiled-coil) antibody, refixed with 3.7% formaldehyde, and incubated with Alexa Fluor 488-conjugated goat anti-rabbit immunoglobulin G. Each set of stained samples was processed under identical gain and laser power settings.

EdU administration and whole-mount detection

EdU (Life Technologies) in PBS was intraperitoneally injected into P21 mice (50 µg/g body weight) once a day for 1 wk. V-SVZ whole mounts were prepared at 2 wk after the final injection and fixed in 100% methanol at −30°C. EdU was detected with a Click-iT EdU Imaging Kit (Life Technologies).

Neurosphere culture from adult mouse V-SVZs

V-SVZs were dissected from 2- to 4-mo-old *Gfap-Cre;Lamc1*$^{cEQ/cEQ}$ mice and their control littermates (*Lamc1*$^{cEQ/cEQ}$ or *Lamc1*$^{cEQ/+}$), mechanically dissociated with a scalpel, incubated in Hank's balanced salt solution containing 12.4 mM $MgSO_4$, 0.01% papain (Worthington Biochemical Co., Lakewood, NJ), 0.01% DNase I (Worthington), and 0.1% Dispase II (Life Technologies) at 37°C, triturated, and washed with DMEM/F12. The cells were resuspended in NeuroBasal medium (Life Technologies) supplemented with N2 (Life Technologies), B27 (Life Technologies), 2 mM L-glutamine, 2 µg/ml heparin, 20 ng/ml basic FGF (Peprotech, Rocky Hill, NJ), 20 ng/ml EGF (Peprotech), and penicillin/streptomycin (Sigma). Viable cells were counted and seeded in non-treated T-25 flasks at a density of 4000 cells/cm^2. At day 7, floating neurospheres were collected in a 15-ml tube, resuspended in 200 µl of Accutase (Innovative Cell Technologies, San Diego, CA), and incubated at 37°C for 10 min. Dissociated neurospheres were resuspended and triturated in 800 µl of medium. An aliquot was counted by trypan blue exclusion assay to determine total viable cells in the primary neurosphere culture.

Statistics

Student's *t* test was performed by Prism 6 (GraphPad software, La Jolla, CA) or Excel (Microsoft, Redmond, WA) software and used in all statistical analyses. Values of $p < 0.05$ were considered significant.

ACKNOWLEDGMENTS

We thank Ri-ichiro Manabe, Ko Tsutsui, and Kenji Kusumoto at the Institute for Protein Research, Osaka University, for their preliminary analysis of the fractone composition and Ryoko Sato-Nishiuchi at the Institute for Protein Research, Osaka University, for her assistance in preparing the original and revised manuscripts. We also thank the NPO Biotechnology Research and Development for technical assistance in generating the *Lama5*^{fl} and *Lamc1*^{cEQ} mice, the National Institutes of Health (NIH) Fellows Editorial Board for editorial feedback on the manuscript, Alison Sherwin from the Edanz Group (www.edanzediting.com/ac) for editing a draft of the manuscript, and Yoh-suke Mukouyama and Robert S. Adelstein at the National Heart, Lung, and Blood Institute, NIH, for assistance in preparing the original and revised manuscripts. This work was supported in part by a Grant-in-Aid for Scientific Research on Priority Areas (#17082005) and a Grant-in-Aid for Scientific Research on Innovative Areas (#22122006) from the Ministry of Education, Culture, Sports, Science and Technology of Japan.

REFERENCES

Adorjan I, Kalman M (2009). Distribution of beta-dystroglycan immunopositive globules in the subventricular zone of rat brain. Glia 57, 657–666.

Allen JM, Brachvogel B, Farlie PG, Fitzgerald J, Bateman JF (2008). The extracellular matrix protein WARP is a novel component of a distinct subset of basement membranes. Matrix Biol 27, 295–305.

Alvarez-Buylla A, Lim DA (2004). For the long run: maintaining germinal niches in the adult brain. Neuron 41, 683–686.

Aumailley M (2013). The laminin family. Cell Adh Migr 7, 48–55.

Bjornsson CS, Apostolopoulou M, Tian Y, Temple S (2015). It takes a village: constructing the neurogenic niche. Dev Cell 32, 435–446.

Codega P, Silva-Vargas V, Paul A, Maldonado-Soto AR, Deleo AM, Pastrana E, Doetsch F (2014). Prospective identification and purification of quiescent adult neural stem cells from their in vivo niche. Neuron 82, 545–559.

Doetsch F (2003). The glial identity of neural stem cells. Nat Neurosci 6, 1127–1134.

Doetsch F, Caille I, Lim DA, Garcia-Verdugo JM, Alvarez-Buylla A (1999). Subventricular zone astrocytes are neural stem cells in the adult mammalian brain. Cell 97, 703–716.

Douet V, Arikawa-Hirasawa E, Mercier F (2012). Fractone-heparan sulfates mediate BMP-7 inhibition of cell proliferation in the adult subventricular zone. Neurosci Lett 528, 120–125.

Douet V, Kerever A, Arikawa-Hirasawa E, Mercier F (2013). Fractone-heparan sulphates mediate FGF-2 stimulation of cell proliferation in the adult subventricular zone. Cell Prolif 46, 137–145.

Hynes RO (2009). The extracellular matrix: not just pretty fibrils. Science 326, 1216–1219.

Ido H, Harada K, Futaki S, Hayashi Y, Nishiuchi R, Natsuka Y, Li S, Wada Y, Combs AC, Ervasti JM, *et al.* (2004). Molecular dissection of the alpha-dystroglycan- and integrin-binding sites within the globular domain of human laminin-10. J Biol Chem 279, 10946–10954.

Ido H, Nakamura A, Kobayashi R, Ito S, Li S, Futaki S, Sekiguchi K (2007). The requirement of the glutamic acid residue at the third position from the carboxyl termini of the laminin gamma chains in integrin binding by laminins. J Biol Chem 282, 11144–11154.

Jacques TS, Relvas JB, Nishimura S, Pytela R, Edwards GM, Streuli CH, ffrench-Constant C (1998). Neural precursor cell chain migration and division are regulated through different beta1 integrins. Development 125, 3167–3177.

Jacquet BV, Salinas-Mondragon R, Liang H, Therit B, Buie JD, Dykstra M, Campbell K, Ostrowski LE, Brody SL, Ghashghaei HT (2009). FoxJ1-dependent gene expression is required for differentiation of radial glia into ependymal cells and a subset of astrocytes in the postnatal brain. Development 136, 4021–4031.

Kazanis I, Lathia JD, Vadakkan TJ, Raborn E, Wan R, Mughal MR, Eckley DM, Sasaki T, Patton B, Mattson MP, *et al.* (2010). Quiescence and activation of stem and precursor cell populations in the subependymal zone of the mammalian brain are associated with distinct cellular and extracellular matrix signals. J Neurosci 30, 9771–9781.

Kerever A, Schnack J, Vellinga D, Ichikawa N, Moon C, Arikawa-Hirasawa E, Efird JT, Mercier F (2007). Novel extracellular matrix structures in the neural stem cell niche capture the neurogenic factor fibroblast growth factor 2 from the extracellular milieu. Stem Cells 25, 2146–2157.

Kerever A, Yamada T, Suzuki Y, Mercier F, Arikawa-Hirasawa E (2015). Fractone aging in the subventricular zone of the lateral ventricle. J Chem Neuroanat 66-67, 52–60.

Kiyozumi D, Sato-Nishiuchi R, Sekiguchi K (2014). In situ detection of integrin ligands. Curr Protoc Cell Biol 65, 10.19.11–10.19.17.

Kiyozumi D, Takeichi M, Nakano I, Sato Y, Fukuda T, Sekiguchi K (2012). Basement membrane assembly of the integrin alpha8beta1 ligand nephronectin requires Fraser syndrome-associated proteins. J Cell Biol 197, 677–689.

Kokovay E, Goderie S, Wang Y, Lotz S, Lin G, Sun Y, Roysam B, Shen Q, Temple S (2010). Adult SVZ lineage cells home to and leave the vascular niche via differential responses to SDF1/CXCR4 signaling. Cell Stem Cell 7, 163–173.

Kriegstein A, Alvarez-Buylla A (2009). The glial nature of embryonic and adult neural stem cells. Annu Rev Neurosci 32, 149–184.

Li J, Tzu J, Chen Y, Zhang YP, Nguyen NT, Gao J, Bradley M, Keene DR, Oro AE, Miner JH, *et al*. (2003). Laminin-10 is crucial for hair morphogenesis. EMBO J 22, 2400–2410.

Liesi P, Silver J (1988). Is astrocyte laminin involved in axon guidance in the mammalian CNS? Dev Biol 130, 774–785.

Lim DA, Tramontin AD, Trevejo JM, Herrera DG, Garcia-Verdugo JM, Alvarez-Buylla A (2000). Noggin antagonizes BMP signaling to create a niche for adult neurogenesis. Neuron 28, 713–726.

Llorens-Bobadilla E, Zhao S, Baser A, Saiz-Castro G, Zwadlo K, Martin-Villalba A (2015). Single-cell transcriptomics reveals a population of dormant neural stem cells that become activated upon brain injury. Cell Stem Cell 17, 329–340.

Manabe R, Tsutsui K, Yamada T, Kimura M, Nakano I, Shimono C, Sanzen N, Furutani Y, Fukuda T, Oguri Y, *et al*. (2008). Transcriptome-based systematic identification of extracellular matrix proteins. Proc Natl Acad Sci USA 105, 12849–12854.

McClenahan FK, Sharma H, Shan X, Eyermann C, Colognato H (2016). Dystroglycan suppresses notch to regulate stem cell niche structure and function in the developing postnatal subventricular zone. Dev Cell 38, 548–566.

Mercier F, Douet V (2014). Bone morphogenetic protein-4 inhibits adult neurogenesis and is regulated by fractone-associated heparan sulfates in the subventricular zone. J Chem Neuroanat 57-58, 54–61.

Mercier F, Kitasako JT, Hatton GI (2002). Anatomy of the brain neurogenic zones revisited: fractones and the fibroblast/macrophage network. J Comp Neurol 451, 170–188.

Merkle FT, Tramontin AD, Garcia-Verdugo JM, Alvarez-Buylla A (2004). Radial glia give rise to adult neural stem cells in the subventricular zone. Proc Natl Acad Sci USA 101, 17528–17532.

Milner R (2007). A novel three-dimensional system to study interactions between endothelial cells and neural cells of the developing central nervous system. BMC Neurosci 8, 3.

Miner JH, Li C, Mudd JL, Go G, Sutherland AE (2004). Compositional and structural requirements for laminin and basement membranes during mouse embryo implantation and gastrulation. Development 131, 2247–2256.

Miner JH, Patton BL, Lentz SI, Gilbert DJ, Snider WD, Jenkins NA, Copeland NG, Sanes JR (1997). The laminin alpha chains: expression, developmental transitions, and chromosomal locations of alpha1-5, identification of heterotrimeric laminins 8-11, and cloning of a novel alpha3 isoform. J Cell Biol 137, 685–701.

Mirzadeh Z, Merkle FT, Soriano-Navarro M, Garcia-Verdugo JM, Alvarez-Buylla A (2008). Neural stem cells confer unique pinwheel architecture to the ventricular surface in neurogenic regions of the adult brain. Cell Stem Cell 3, 265–278.

Nascimento MA, Sorokin L, Coelho-Sampaio T (2018). Fractone bulbs derive from ependymal cells and their laminin composition influence the stem cell niche in the subventricular zone. J Neurosci 38, 3880–3889.

Nishiuchi R, Takagi J, Hayashi M, Ido H, Yagi Y, Sanzen N, Tsuji T, Yamada M, Sekiguchi K (2006). Ligand-binding specificities of laminin-binding integrins: a comprehensive survey of laminin-integrin interactions using recombinant alpha3beta1, alpha6beta1, alpha7beta1 and alpha6beta4 integrins. Matrix Biol 25, 189–197.

North HA, Pan L, McGuire TL, Brooker S, Kessler JA (2015). beta1-Integrin alters ependymal stem cell BMP receptor localization and attenuates astrogliosis after spinal cord injury. J Neurosci 35, 3725–3733.

Ottone C, Krusche B, Whitby A, Clements M, Quadrato G, Pitulescu ME, Adams RH, Parrinello S (2014). Direct cell-cell contact with the vascular niche maintains quiescent neural stem cells. Nat Cell Biol 16, 1045–1056.

Rietze RL, Reynolds BA (2006). Neural stem cell isolation and characterization. Methods Enzymol 419, 3–23.

Riquelme PA, Drapeau E, Doetsch F (2008). Brain micro-ecologies: neural stem cell niches in the adult mammalian brain. Philos Trans R Soc Lond B Biol Sci 363, 123–137.

Robel S, Mori T, Zoubaa S, Schlegel J, Sirko S, Faissner A, Goebbels S, Dimou L, Gotz M (2009). Conditional deletion of beta1-integrin in astroglia causes partial reactive gliosis. Glia 57, 1630–1647.

Rousselle P, Beck K (2013). Laminin 332 processing impacts cellular behavior. Cell Adh Migr 7, 122–134.

Sato Y, Uchida Y, Hu J, Young-Pearse TL, Niikura T, Mukouyama YS (2017). Soluble APP functions as a vascular niche signal that controls adult neural stem cell number. Development 144, 2730–2736.

Sato-Nishiuchi R, Nakano I, Ozawa A, Sato Y, Takeichi M, Kiyozumi D, Yamazaki K, Yasunaga T, Futaki S, Sekiguchi K (2012). Polydom/SVEP1 is a ligand for integrin alpha9beta1. J Biol Chem 287, 25615–25630.

Schneider CA, Rasband WS, Eliceiri KW (2012). NIH image to ImageJ: 25 years of image analysis. Nat Methods 9, 671–675.

Shen Q, Wang Y, Kokovay E, Lin G, Chuang SM, Goderie SK, Roysam B, Temple S (2008). Adult SVZ stem cells lie in a vascular niche: a quantitative analysis of niche cell-cell interactions. Cell Stem Cell 3, 289–300.

Silva-Vargas V, Crouch EE, Doetsch F (2013). Adult neural stem cells and their niche: a dynamic duo during homeostasis, regeneration, and aging. Curr Opin Neurobiol 23, 935–942.

Smyth N, Vatansever HS, Murray P, Meyer M, Frie C, Paulsson M, Edgar D (1999). Absence of basement membranes after targeting the LAMC1 gene results in embryonic lethality due to failure of endoderm differentiation. J Cell Biol 144, 151–160.

Staquicini FI, Dias-Neto E, Li J, Snyder EY, Sidman RL, Pasqualini R, Arap W (2009). Discovery of a functional protein complex of netrin-4, laminin gamma1 chain, and integrin alpha6beta1 in mouse neural stem cells. Proc Natl Acad Sci USA 106, 2903–2908.

Tavazoie M, Van der Veken L, Silva-Vargas V, Louissaint M, Colonna L, Zaidi B, Garcia-Verdugo JM, Doetsch F (2008). A specialized vascular niche for adult neural stem cells. Cell Stem Cell 3, 279–288.

Yousif LF, Di Russo J, Sorokin L (2013). Laminin isoforms in endothelial and perivascular basement membranes. Cell Adh Migr 7, 101–110.

Yurchenco PD, Amenta PS, Patton BL (2004). Basement membrane assembly, stability and activities observed through a developmental lens. Matrix Biol 22, 521–538.